Int. J. Electrochem. Sci., 12 **(2017)** 5539 – 5552, doi: 10.20964/2017.06.25

International Journal of
ELECTROCHEMICAL
SCIENCE
www.electrochemsci.org

Effect of Sustained Load on the Passive Film of Carbon Steel Embedded in Concrete

Sen Pang[1,*], *Bo Diao*[1,2], *Yinghua Ye*[1]

[1] School of Transportation Science and Engineering, Beihang University, Beijing 100191, China.; pang.sn@buaa.edu.cn(S.Pang);diaobo@buaa.edu.cn(B.Diao);yhye@buaa.edu.cn(Y.H.Ye);
[2] State Laboratory of Subtropical Building Science, South China University of Technology, Guangzhou 510640, China.
[*]E-mail: pang.sn@buaa.edu.cn

Received: 6 March 2017 / *Accepted:* 11 April 2017 / *Published:* 12 May 2017

Reinforced concrete structures experience different kinds of load, which may influence the passive behaviour of steel. For the purpose of simulating in-service condition, the steel sample for electrochemical measurement was embedded in concrete in this study. The effects of sustained load level and duration on the passive behaviour of carbon steel were studied via electrochemical impedance spectroscopy. The protective effect of passive film decreased as the load level increased. A re-passivation kinetics was detected during sustained loading. The degree of re-passivation decreased when the load level increased. A peak of re-passivation was observed after the load was sustained for 24h. Electrochemical measurement applied on steel embedded in concrete offers the possibility of non-destructive testing in reinforced concrete structures.

Keywords: Steel reinforced concrete; EIS; Passive films; Re-passivation; Effects of strain;

1. INTRODUCTION

The steel bar in concrete is protected by a passive film formed under the alkaline condition of concrete (pH 12–13). However, the passive film may be damaged by an aggressive medium, such as chloride, atmospheric carbonation and load. Passivation and de-passivation of steel play a great role in corrosion process. The breakdown of passive film will accelerate the corrosion process of steel bar in concrete. Many studies on de-passivation and re-passivation of steel were conducted. Saremi et al. [1] found a severe decrease in resistance of interfacial reaction, which meant the breakdown of passive film when the $[Cl^-]/[OH^-]$ ratio was above 0.6 in simulated concrete pore solution. Zhao et al. [2] found that steel embedded in mortar after 3.5% NaCl drying-wetting cycles had three corrosion stages, a

competition process between breakdown and re-passivation of passivation film, a pitting development and an active corrosion process. Lin and Xu [3] investigated the corrosion behavior of fine-grain high-strength reinforcement in simulated concrete pore solutions with various $[NO^{2-}]/[Cl^{-}]$ ratios. Results showed that the corrosion resistance improved in the presence of nitrite. Reffass et al. [4, 5] investigated the effect of nitrite ions and phosphate ions on corrosion process of carbon steel in $NaHCO_3$+NaCl solution and found that nitrite ions were efficient inhibitors of the corrosion of steel reinforcement in concrete and the re-passivation was completely associated with oxidizing action of nitrite ions. In contrast with nitrite ions, the addition of phosphate ions did not lead to the re-passivation of steel inside well-grown pits. Tang et al. [6] found that sodium molybdate, sodium tungstate and sodium nitrite revealed effective inhibition effects by promoting passivation of the steel. Dong et al. [7] found nitrite and TEPA can accelerate the rehabilitation process of metastable pits, resulting in an increase of pitting corrosion resistance of carbon steel. In contact with a high alkaline environment, carbon steel can attain a very stable passive state [8, 9] and may be re-passivated under certain circumstance [10].

The reinforced concrete structure in working condition suffers different kinds of load, such as cycle load, fatigue load and sustained load, and may affect the passive behaviour of steel bars embedded in concrete. Feng et al. [10, 11, 12] studied the effect of stress on passivation of steel bar in pore solution. The results showed that the passive ability of the steel in pore solution decreased as the applied load increased. Zhu et al. [13] studied the effects of tensile stress on the oscillatory electrodissolution of X70 carbon steel in sulfuric acid solution and found that the tensile stress degrades the stability and increases the defects of passive film. Jiang et al. [14] discovered that the chloride threshold value first increased and then decreased with increasing fatigue cycle times under a certain stress level and number of cracks on passive film. Zhang and Poursaee [15, 16] studied the passivation behaviour of carbon steel and semi-conductive behaviour of passive film on carbon steel in simulated concrete pore solution under stress. The results showed that the passive film formed under tensile condition is more protective compare to that under compressive loading conditions in chloride-free pore solution. Liu et al. [17] studied electrochemical impedance spectroscopy characteristic of Ti6Al-4V alloy under the different load and results showed that the load stress reduced the oxide film resistance, which indicated that the integrality of the oxide film was destroyed. In the study of Li et al. [18], the intergranular stress corrosion cracking of sensitized 304 stainless steel in $Na_2S_2O_3$ solution was detected by electrochemical noise and acoustic emission techniques. Results showed that, under the elastic deformation, the passive film on sensitized 304 stainless steel especially at the sensitized grain boundaries would be firstly broken down and then re-passivated again.

Most studies on passive behaviour of steel were performed in saturated $Ca(OH)_2$ solution or simulated concrete pore solution. However, for reinforced concrete structures, steel bars were embedded in concrete, and tensile cracks were induced by service load. Thus, the working conditions of steel bars to become passivated are different from the conditions of saturated $Ca(OH)_2$ solution or simulated concrete pore solution. Ghods et al. [19] studied the effect of cations on passive film grown in saturated $Ca(OH)_2$ solution. The results showed that Na^{+}, K^{+} and Ca^{2+}, which were commonly observed in most ordinary Portland cement, could affect the passive film formed on steel. In particular, SO_4^{2-} ion in pore solution had a significant negative effect on the protective properties of passive film.

Zhu et al. [20] studied the effect of chloride salt type on the chloride binding capacity of concrete and found that the chloride binding capacity varied with the chloride cation type as Ca^{2+}>Mg^{2+}>Na^{+}. Duarte et al. [21] studied the electrochemical behaviour of stainless steels by electrochemical impedance spectroscopy when embedded in concrete specimens and found that the use of stainless steel rebars provided a strong increase of the corrosion resistance when concrete specimens in contact with chlorides. Yang et al. [22] studied the general corrosion processes of mild steel caused by the introduction of chloride ions and sulfate ions in simulated marine environment and results showed that in simulated marine environment sulfate ions only had slight influence for the passive film compared to chloride ions which could rapidly destroy the passive film on the steel surface.

The disadvantage of simulating the working environment in pore solution was that the passivation evolution on the surface of steel bar covered by concrete cannot be replicated in pore solution [23]. In the site condition, many factors influence the situation of the passive film, including the following: (1) type of cement [24]; (2) concrete additive [25-27]; (3) water/cement ratio [28]; (4) surface finishing and metallurgical composition of steel bars [29]; and (5) level of loading damage. In this study, for the purpose of simulating the real working condition of reinforced concrete structures, the steel bar was embedded in concrete and not in simulated pore solution to investigate the effect of sustained load level and load duration on the passive behaviour of steel bar. A self-designed device was used in the experiment for applying and sustaining loads.

2. EXPERIMENTAL METHODS

2.1 Preparation of carbon steel bars

The steel for the test was a hot rolled ribbed bar with 10 mm in diameter, and all bars were from the same batch. The Young's modulus of the steel bar was 2.03×10^5 MPa, and its yield strength was 350 MPa. The chemical composition (wt. %) of the steel bars is shown in Table 1. The steel bar was cut into segments with length of 450 mm and was bended at right angle at both ends for good bond between concrete and bar. The middle segment of the steel bar was grinded on an emery wheel machine to grind off ribs and formed a platform. The platform was abraded with silicon carbide abrasive paper to No. 800, degreased by rinsing with acetone, and dried in air. A strain gauge of 1×2 mm was stick on the platform of steel bar to test the tensile strain. A copper wire was soldered to the end of the steel bar for electrochemical testing. The surface of the steel bar platform had an exposed area of about 1 cm^2, and the remaining areas of the bar were sealed by silica gel, as shown in Figure 1. The prepared steel bars subsequently embedded in concrete were used as working electrode in electrochemical measurements. All chemical reagents applied in this study were of analytical reagent grade.

Table 1. Chemical composition of the steel rebar (mass fraction, %).

C	Mn	S	P	Si	V	Fe
0.21	1.37	0.023	0.031	0.46	0.029	Balance

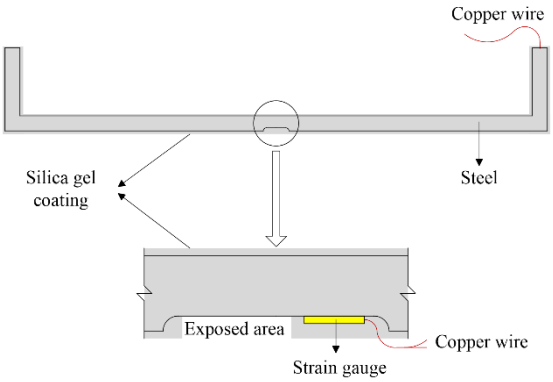

Figure 1. Illustration of the prepared carbon steel bar and enlarged image of the middle segment.

2.2. Reinforced concrete beam specimens

The mixture proportions of concrete are listed in Table 2. Ordinary Portland cement, deionized water and naphthalene series water reducing agent were used. The chemical composition of cement is presented in Table 3. The maximum size of coarse aggregate was about 8-10 mm and the fineness modulus of fine aggregate was 2.2 with the soil content less than 1%. The coarse aggregate and fine aggregate were rinsed with distilled water before mixing. All the materials were free from chlorides, especially the water. After an appropriate mixing, concrete beam specimens of 100 mm × 100 mm × 400 mm were cast, and one prepared steel bar was embedded in the beam specimen as reinforcement. A sketch of the reinforced concrete beam specimen is shown in Figure 2. The thickness of concrete cover was 30 mm.

Table 2. Mixture proportion of concrete (kg/m3).

Materials	Ordinary Portland Cement	Deionized Water	Fine Aggregate	Coarse Aggregate	Water reducing agent	w/c
Volume	560	250	660	990	8L	0.45

Table 3. Chemical composition of cement (mass fraction, %. LoI: loss of ignition).

CaO	SiO_2	MgO	Al_2O_3	Na_2O	Fe_2O_3	K_2O	SO_3	LoI
63.27	21.96	2.18	4.30	0.20	3.42	0.33	2.68	1.54

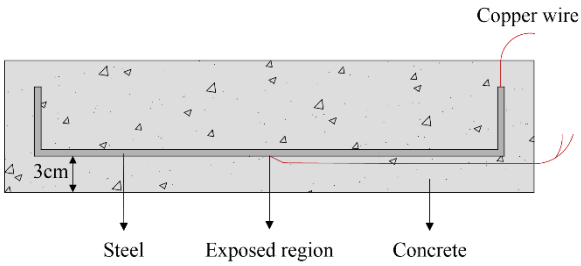

Figure 2. Concrete specimen with the prepared steel bar as reinforcement and position of exposed region without silica gel coating for tests.

The paired copper line, which was soldered to the strain gauge in the middle of the steel bar, was used to establish conduction with a dynamic resistance strain instrument. Test cubes of 100 mm for compressive strength test were made from the same concrete mixture. Specimens were cured in a 90% RH atmosphere at 25±1 °C for 28 days. After 28 days, concrete compressive strength measurement was conducted on test cubes, according to the Chinese standard GB/T 50081-2002 ("Standard for Test Method of Mechanical Properties on Ordinary Concrete").The compressive strength of concrete was 55MPa. Different strain values were designed to applied to the steel rebar beam specimen (i.e., 250, 500, 750, 1000, 1250, 1500, 1750 and 2000×10^{-6}, respectively, corresponding to stress value of 50, 100, 150, 200, 250, 300 and 350 MPa). Each test had three parallel specimens to verify the reproducibility.

2.3 Measurement methods

All the electrochemical measurements were conducted at 25°C with a platinum plate of 8 cm × 8 cm as counter electrode and a saturated calomel electrode (SCE) as reference electrode. Electrochemical impedance spectra (EIS) measurements were performed at PAR VersaSTAT MC electrochemical workstation. A sinusoidal potential disturbance of 10 mV was applied at the open circuit potential (OCP) with frequency sweep ranging from 10^5 Hz to 10^{-2} Hz. EIS was performed as two-point measurements. The reference and counter electrodes were short-circuited and then connected to the platinum plate; the working electrode was connected to the steel bar (see Figure 4).

The OCP measurement was conducted with a high precision voltmeter. The reinforced concrete specimen and the OCP measurement setup were assembled together, as illustrated in Figure 3. The difference of potential value between the SCE and the steel embedded in concrete was measured by the high precision voltmeter.

A dynamic resistance strain instrument was applied to obtain the strain of the reinforcing steel caused by sustained load with a sampling frequency of 2000 Hz.

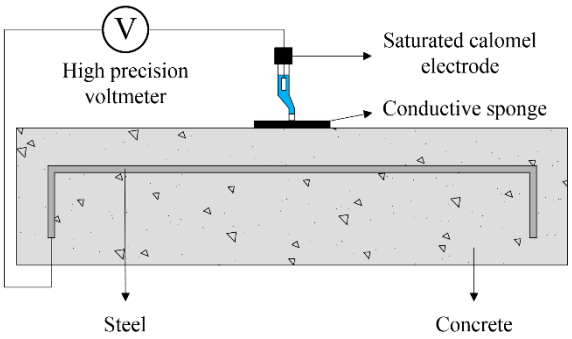

Figure 3. Sketch of experimental setup for OCP measurement.

2.4 Experimental procedure

The reinforced concrete beam specimen was loaded by a self-designed loading device, as shown in Figure 4. As bolts were tightened, a vertical load was applied to the beam specimen. Therefore, the steel bar in the bottom of beam was in tension. The tensile strain of the steel bar was monitored by a dynamic strain instrument, and the strain was controlled by tightening degree of bolts. According to the tensile test result of the steel bars, a plastic deformation appeared when the strain exceeded 1700×10^{-6}. As long as bolts remained tightened, the load on the concrete would be sustained.

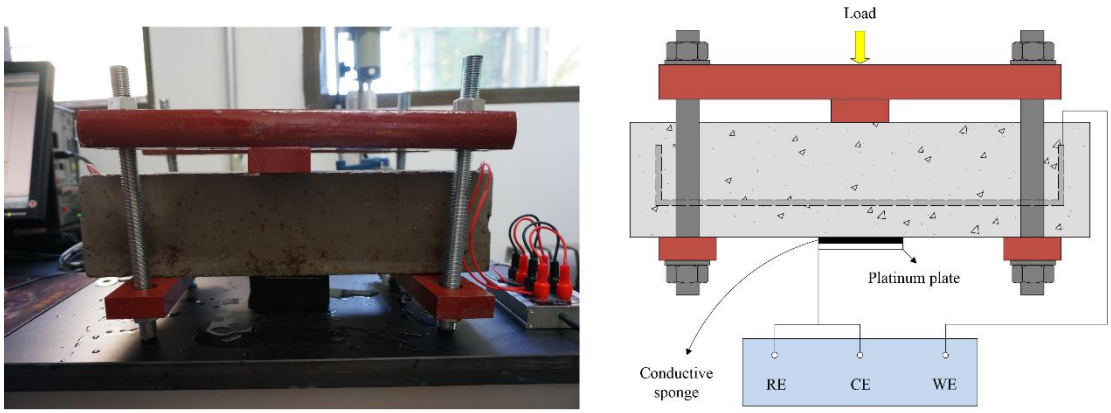

Figure 4. (a) Schematic of self-designed sustaining load device. (b) Setup for electrochemical impedance spectra measurement.

During reinforced concrete beam specimen curing, OCP monitoring was performed on each beam specimen every day to observe the formation of passive film on the steel bar embedded in concrete. Prior to electrochemical measurement, beam specimens were immersed in water for 3 days to form a water-saturated condition inside the concrete. Subsequently, specimens together with the loading devices were moved into a thermostatic control chamber to ensure that the temperature and humidity were same for every EIS measurement. Different strain values were applied to the steel rebar beam specimen (i.e., 250, 500, 750, 1000, 1250, 1500, 1750 and 2000×10^{-6}, respectively,

corresponding to stress value of 50, 100, 150, 200, 250, 300 and 350 MPa). EIS measurement was conducted at each load level. The load on the beam specimen lasted for 3, 6, 12, 24, 48 and 72 h to study the effect of sustained load on passive behaviour. EIS measurement was conducted at the time point mentioned above. Except during loading and EIS testing, specimens along with the loading devices were immersed in water to ensure that the water content of concrete is steady.

3. RESULTS AND DISCUSSION

3.1 Testing results of OCP

Figure 5 shows the OCP value of the steel bar embedded in concrete during curing. As shown in Figure 5, the OCP value increased rapidly in the first 12 h from pouring completion and exhibited a significant negative shift during the next 60 h. The value rises again in the next 48 h, became more anodic gradually and remained stable relatively thereafter. This trend was similar to the testing results from Poursaee et al. [30] and Narvaez et al. [31]. The variation of OCP indicated that the passive film was being developed.

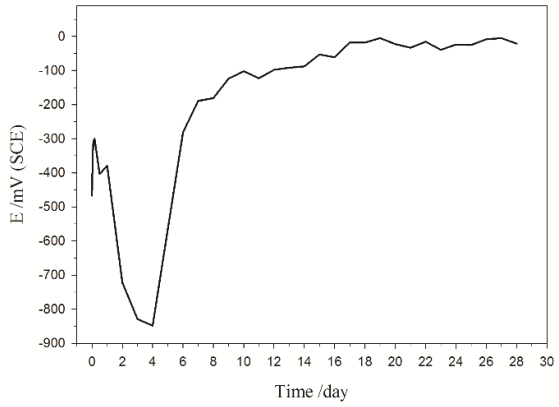

Figure 5. OCP value of the steel bar embedded in concrete for 28 days.

After the beam specimens were cast, the OCP of steel bars decreased during the first 3 days, increased rapidly and then remained in a relatively high level for 28 days. This change was considered a change in permittivity of the mortar as it set and hardened. Poursaee et al. [30] found a similar phenomenon. Other studies that conducted the passivation process in saturated $Ca(OH)_2$ solution or simulated concrete pore solution did not report such anomalous behaviour of potential. Different studies found that the duration of steel to be passive differs. Poursaee et al. [30] reported that steel took about 3 days to be passively immersed in saturated $Ca(OH)_2$, whereas it would take 7 days to be embedded in concrete. Ghods et al. [19] reported that steel required 8 days at least to obtain a stable passive film on as-received steel rebar via immersion in saturated $Ca(OH)_2$ solution. In this study, the steel bar was embedded in concrete for 28 days before testing, giving it enough time to be passive. The testing results from OCP (Figure 5) and EIS (Figure 7) indicate that the passive film was formed on the steel after 28 days of curing.

A difference in the OCP value between the end time of curing and the start time of loading can be observed in Figure 5 and Figure 8. This difference could be explained by the change in resistance of concrete due to the variation of water-saturated degree. The water content had a great effect on concrete resistance, and a higher water content of concrete would result in a lower resistance. This finding could be proved by the study [32] that found that the concrete resistance decreased obviously as water content increased. In this study, concrete specimens were immersed in water for 3 days to form a water-saturated condition inside the concrete. Therefore, a decrease of concrete resistance produced a voltage drop, which was equivalent to a decrease in internal resistance of source in circuit. The voltage drop resulted in the difference of the OCP value between the end time of curing and the start time of loading.

3.2 Electrochemical impedance spectroscopy (EIS)

All the impedance spectra presented resistance behaviour in high frequency and capacity behaviour in low frequency at the initial time. As a result of three-point bending, the concrete beam cracked in the tension zone. Thus, water uptake in the cracked regions would lead to the change of electrical properties of cracked concrete and affected the electrochemical measurement which resulted in the irregular impedance data in high frequency. Therefore, an equivalent circuit [33] (see Figure 6) was applied to analyse the impedance data with Zsimpwin software. In the equivalent circuit, R_s is the solution resistance; R_c and Q_c are the resistance and capacitance of the concrete cover, respectively; and R_p and Q_{dl} represent the polarisation resistance and the double-layer capacitance, respectively. The equivalent circuit fits the impedance data well. The value of chi-squared is less than 1×10^{-3}, and the relative error of polarisation resistance is less than 10%. A constant phase element (CPE) is used to represent the double-layer capacity instead of a pure capacitance. The impedance of CPE is given by

$$Z_{CPE} = \left[Q(j\omega)^n \right]^{-1} \quad (1)$$

where parameter n is the CPE exponent. The CPE-like response is due to the charging of a discontinuous and inhomogeneous interface [33]. The CPE will be pure capacitance and pure resistance when n=1 and n=0, respectively. Parameter n ranged from 0.5 to 0.65, which is obtained by fitting the experimental impedance data in this research.

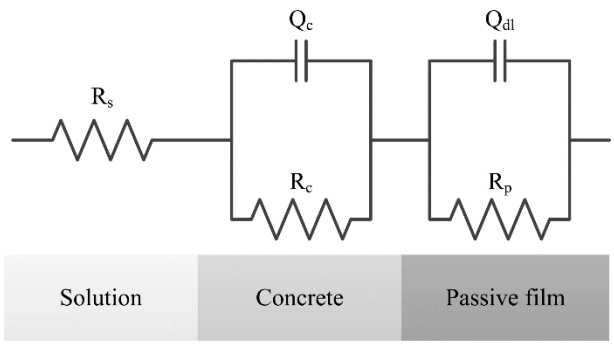

Figure 6. Equivalent electrical circuit applied to analyse impedance data.

3.2.1 Effect of load level

After 28 days of curing, loads with different level, expressed as stress levels 50, 100, 150, 200, 250, 300 and 350 MPa, were applied on the beam specimen. Figure 7 shows the Bode plots of the steel bars embedded in concrete. When the highest load (350 MPa) was applied, a plastic deformation appeared, and the strain increased to 1900×10^{-6} and then remained stable. As shown in Figure 7, the impedance modulus of the loaded beam specimen decreased obviously compared with that of the specimen without load and decreased with the increase of load level. Figure 8 shows the variation of the OCP value of the steel bar embedded in concrete as the strain changed. Figure 8 shows that the potential tended to be more negative with the increase of strain. This finding indicated that the passive film would be damaged more severely when the strain of the steel bar was larger or when the beam specimen suffered a higher load.

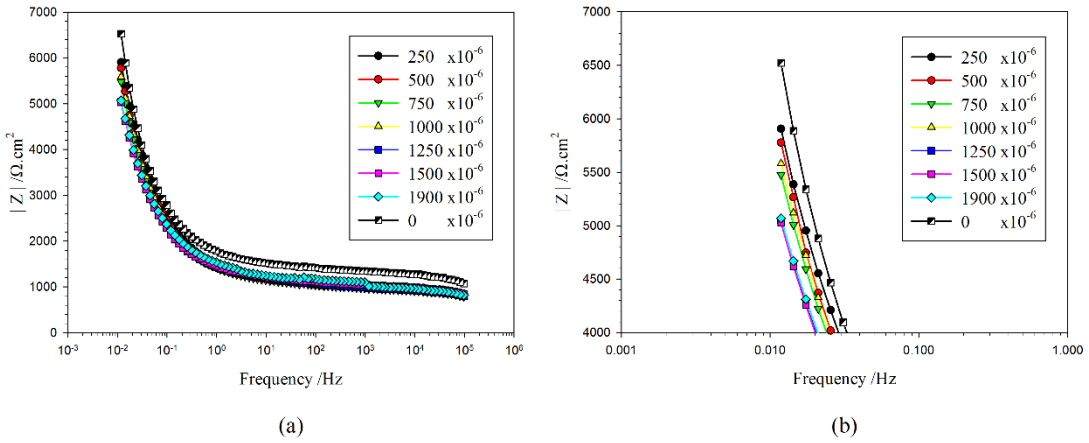

Figure 7. Bode plots of the steel bar embedded in concrete with different strain level: (a) Bode plots and (b) magnification of low frequency part.

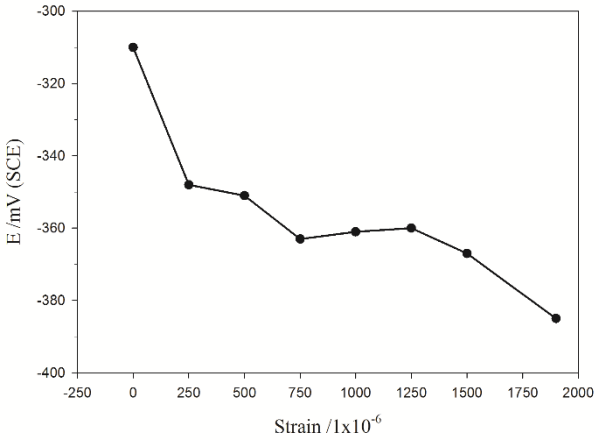

Figure 8. OCP variation of the steel bar embedded in concrete with strain.

Figure 9 shows the variation of R_p and Q_{dl} values. As shown in Figure 9, the polarisation resistance R_p decreased obviously when the tension strain of steel bar was small. The value of R_p

decreased with the increase of tension strain, but the decrease extent reduced gradually. The double-layer capacitance Q_{dl} exhibited a contrary trend, where the value of Q_{dl} increased as tension strain increased. The protective effect of passive film can be related to its thickness and consequently to C (equivalent to Q value of CPE) [34]:

$$C = (\varepsilon \cdot \varepsilon_0) / d \qquad (2)$$

In the above formula, ε and ε_0 are dielectric constants of the passive film and vacuum, respectively, and d is thickness of the passive film. From the formula, the decrease of passive film thickness leads to an increase of C value.

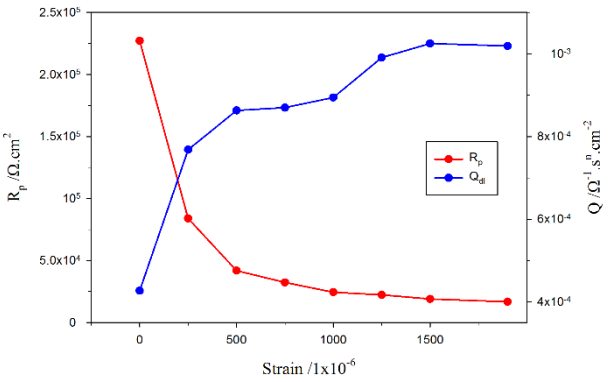

Figure 9. R_p and Q_{dl} of steel bar with different strains.

As shown in Figure 9, the value of Q_{dl} increased as strain increased, which indicated that the thickness of passive film decreased and the resulting protective capacity reduced when the load level of reinforced concrete beam specimen gradual increased. The variation of polarisation resistance and double-layer capacitance value illustrated that the higher load level applied on the beam specimen, the more severely passively damaged the film was. Furthermore, when the strain of steel bar was comparatively small, a relatively large reduction in protective capacity was produced. Most of the passive film damage occurred in the low strain stage (less than 1000×10^{-6}, corresponding to 200 MPa), in which the steel deformed elastically. However, an inconspicuous change in R_p and Q_{dl} was observed when the steel deformed from elastically to plastically (1500×10^{-6} to 1900×10^{-6}, plastic deformation appeared above 1700×10^{-6}).

3.2.2 Effect of load duration

Figure 10 depicts the Nyquist plots of steel bars embedded in concrete beams under different load levels and different load durations, where load level was expressed as tension strain values of 750, 1250, 1500 and 1900×10^{-6}, and the load duration ranged from 0 h to 72 h. The Nyquist plots of the steel bar that experienced the highest load are shown in Figure 10(d); in this figure, the strain of the steel bar was 1900×10^{-6} and plastic deformation occurred. Figure 10(d) shows that the diameter of capacity arc increased gradually with the increase of load duration. After the load was sustained for 12

h, the diameter of capacity arc became steady, and Nyquist plots almost overlapped. However, the curve of 72 h decreased compared with that of 48 h, and a similar phenomenon appeared when the strain was 1500 and 1250×10^{-6}, as shown in Figure 10(b), (c). In the lower load level, Nyquist plots (Figure 10(a)) showed a similar trend as that in the higher load level, but the variation among curves was less than that in the higher load level.

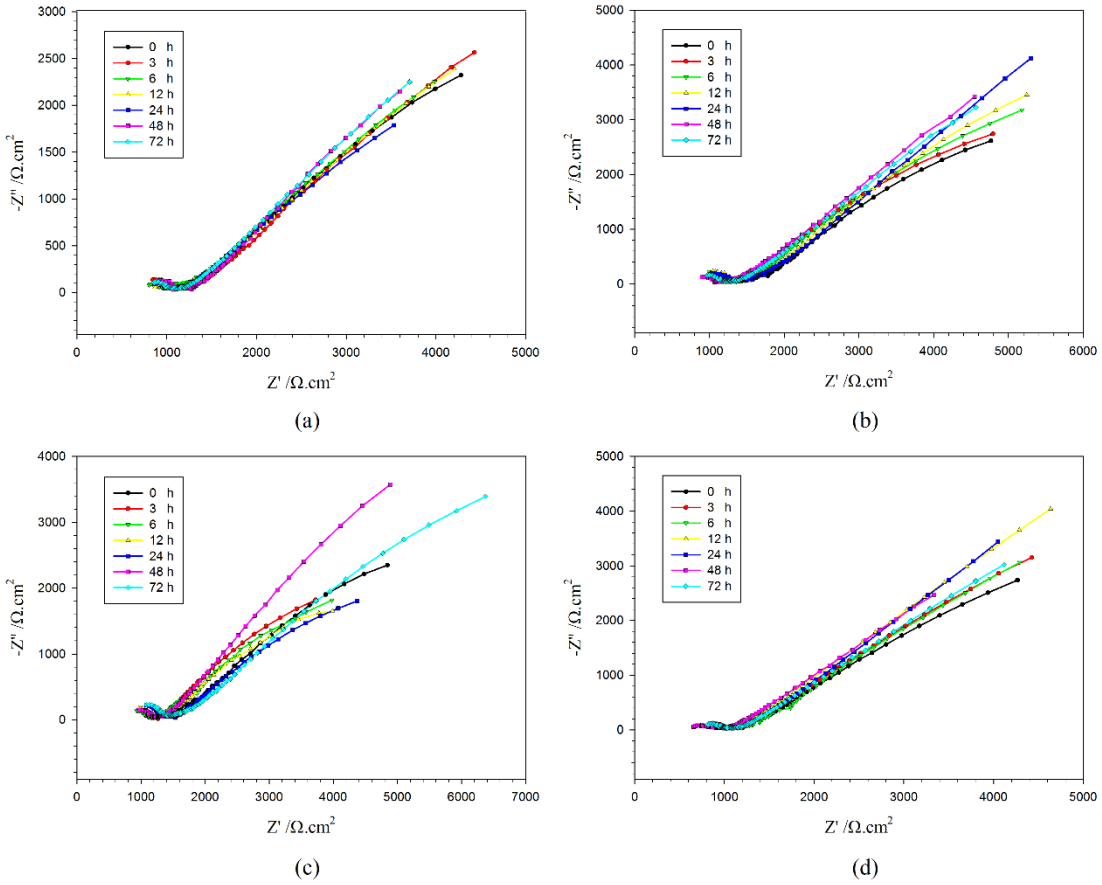

Figure 10. Nyquist plots of steel bar with different load durations and strain. (a) 750, (b) 1250, (c) 1500 and (d) 1900×10^{-6}.

Reinforced concrete structures in service condition will bear different levels of loads, which would last for a long time. Figure 11 shows the fitting results of impedance data by the same equivalent circuit. Many researchers [35-38] found that the alkalinity of concrete would remain in a high level for some time. This phenomenon may provide a high alkaline environment for the steel embedded in concrete to be passivated again (re-passivated). Figure 11 shows that all the plots show a similar tendency to be re-passivated in the first 24 h since application of different level of loads (750, 1250, 1500 and 1900×10^{-6}, corresponding to 150, 250, 300 and 350 MPa). However, the re-passivation kinetics was not monotonous, and peak and valley values of R_p and Q_{dl} were found, respectively. As shown in Figure 11(a), an extremum value of R_p and Q_{dl} was found after the load had been sustained for 3 h, which indicated the existence of a peak of re-passivation.

However, as the load duration increased, the protective ability decreased again. A similar phenomenon is shown in plots (b), (c) and (d), but the appearance of peak value was later than that in low load level (150 MPa). In higher load levels (i.e., 250, 300 and 350 MPa), the maximum of re-passivation appeared between 24 and 48 h after loading, and the degree of re-passivation was lower than that in low load level. Figure 11 shows that the value of R_p and Q_{dl} changed obviously from the non-loading to initial loading and illustrates the damage of passive film.

The peak of re-passivation may be explained by oversized cracks, which established an access to the external neutral environment and hence lowered the pH value of the crack zone. The lower pH value results in a reduction of passivated ability [39-42]. The higher load level applied on the RC beam, the wider the crack was and the more external environment matter transferred into concrete. The load can cause a damage of the passive film (Figure 7 and Figure 8) and reduces the capacity of re-passivation (Figure 11). This finding can be explained by the micro-cracks on the passive film [10, 11, 14]. The oversized cracks and too-large strains (corresponding to load) caused reduction of re-passivation and increase of re-passivated time, as illustrated in Figure 11. For in-service reinforced concrete structures, loads can reduce the protective effect of passive film, but will be almost re-passivated under smaller loads. The degree of re-passivation decreased as the load level increased.

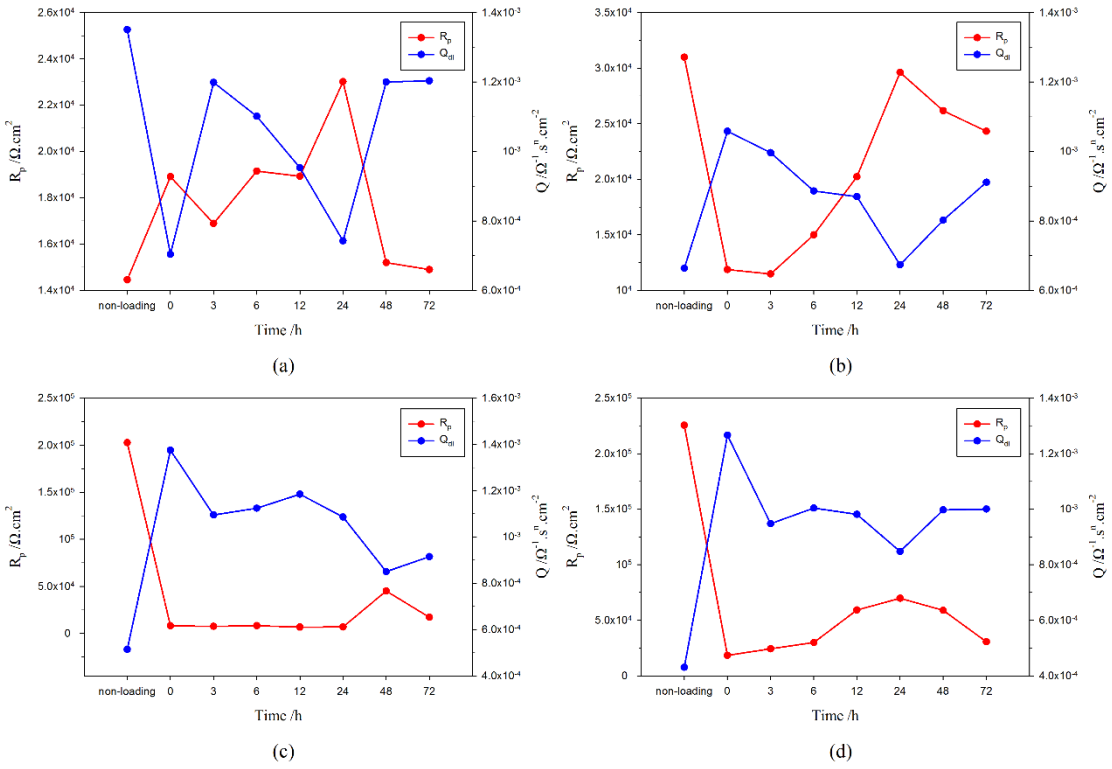

Figure 11. Variation of R_p and Q_{dl} of steel bar with load duration: (a) 750, (b) 1250, (c) 1500 and (d) 1900×10^{-6}.

4. CONCLUSIONS

Passive film can be damaged by external load, and the protective effect decreased as the load level increased. The damage of passive film occurred mostly in the elastic deformation stage of steel

bars embedded in concrete beams. A re-passivation kinetics was detected when the load was sustained. The steel bar embedded in concrete beam can be re-passivated due to the high alkaline environment of concrete. The effect of re-passivation decreases as the tensile strain of the steel bar increases. The 72 h value of double-layer capacitance Q_{dl} (relate to the thickness of passive film) can reach 60–80% of the non-loading value in higher load levels (the tensile strains are 1250 and 1500×10^{-6}, corresponding to 250 and 300 MPa, respectively). Plastic deformation makes the steel bar more difficult to be re-passivated. A peak value of R_p and a valley value of Q_{dl} appear when the load has been sustained for about 24 h. This peak value may be caused by oversized cracks, which establish an access to the external neutral environment and hence lower the local pH value.

-

ACKNOWLEDGEMENTS

This work was financially supported by National Natural Science Foundation of China (51578031) and the Open Project of State Key Laboratory of Subtropical Building Science, South China University of Technology (2016ZA03).

Conflicts of Interest

The authors declare that they have no conflict of interest.

References

1. M. Saremi and E. Mahallati, *Cem. Concr. Res*., 32 (2002) 1915-1921.
2. B. Zhao, J. H. Li, R. G. Hu, R. G. Du and C. J. Lin, *Electrochim. Acta*, 52 (2007) 3976-3984.
3. B. L. Lin and Y. Y. Xu, *Int. J. Electrochem. Sci.*, 11 (2016) 3824-3842.
4. M. Reffass, R. Sabot, M. Jeannin, C. Berziou and P. Refait, *Electrochim. Acta*, 52 (2007) 7599-7606.
5. M. Reffass, R. Sabot, M. Jeannin, C. Berziou and P. Refait, *Electrochim. Acta*, 54 (2009) 4389-4396.
6. Y. M. Tang, G. D. Zhang and Y. Zuo, *Constr. Build. Mater*., 28 (2012) 327-332.
7. Z. H. Dong, W. Shi, G. A. Zhang and X. P. Guo, *Electrochim. Acta*, 56 (2011) 5890-5897.
8. M. B. Valcarce and M. Vazquez, *Electrochim. Acta*, 53 (2008) 5007-5015.
9. D. Z. Tang, Y. X. Du, M. X. Lu, Y. Liang, Z. T. Jiang and L. Dong, *Mater. Corros*., 66 (2015) 1467-1479.
10. X. G. Feng, Y. M. Tang and Y. Zuo, *Corros. Sci*., 53 (2011) 1304-1311.
11. X. G. Feng, Y. Zuo, Y. M. Tang, X. H. Zhao and X. Y. Lu, *Electrochim. Acta*, 58 (2011) 258-263.
12. X. G. Feng, X. Y. Lu, L. Q. Guo and D. Chen, *Int. J. Electrochem. Sci.*, 10 (2015) 10677-10688.
13. Y. Y. Zhu, L. Li and C. Wang, *Corrosion Sci*., 94 (2015) 445-451.
14. L. H. Jiang, H. Liu, H. Q. Chu, C. L. Zhu, C. S. Xiong, L. S. You, J. X. Xu, Y. Zhang and Y. J. Qin, *Constr. Build. Mater*., 73 (2014) 699-704.
15. Y. Zhang and A. Poursaee, *J. Mater. Civ. Eng*., 27 (2015) 9.
16. Y. J. Zhang and A. Poursaee, *Anti-Corros. Methods Mater*., 62 (2015) 363-370.
17. Y. Liu, S. W. Tang, G. Y. Liu, Y. Sun and J. Hu, *Int. J. Electrochem. Sci.*, 11 (2016) 8530-8545.
18. B. Li, J. H. Wang, X. H. Wang and X. Yue, *Int. J. Electrochem. Sci.*, 11 (2016) 1-13.
19. P. Ghods, O. B. Isgor, G. McRae and T. Miller, *Cem. Concr. Compos*., 31 (2009) 2-11.
20. Q. Zhu, L. H. Jiang, Y. Chen, J. X. Xu and L. L. Mo, *Constr. Build. Mater*., 37 (2012) 512-517.
21. R. G. Duarte, A. S. Castela, R. Neves, L. Freire and M. F. Montemor, *Electrochim. Acta*, 124

(2014) 218-224.
22. L. J. Yang, Y. Z. Xu, Y. S. Zhu, L. Liu, X. N. Wang and Y. Huang, *Int. J. Electrochem. Sci.*, 11 (2016) 6943-6958.
23. T. D. Marcotte and C. M. Hansson, *Mater. Struct*., 40 (2007) 325-340.
24. C. Arya and Y. Xu, *Cem. Concr. Res*., 25 (1995) 893-902.
25. M. Thomas, *Cem. Concr. Res*., 26 (1996) 513-519.
26. B. Pacewska, M. Bukowska, I. Wilinska and M. Swat, *Cem. Concr. Res*., 32 (2002) 145-152.
27. D. M. Bastidas, A. Fernandez-Jimenez, A. Palomo and J. A. Gonzalez, *Corrosion Sci*., 50 (2008) 1058-1065.
28. W. Morris and M. Vazquez, *Corros. Rev*., 20 (2002) 469-508.
29. L. T. Mammoliti, L. C. Brown, C. M. Hansson and B. B. Hope, *Cem. Concr. Res*., 26 (1996) 545-550.
30. A. Poursaee and C. M. Hansson, *Cem. Concr. Res*., 37 (2007) 1127-1133.
31. L. E. Narvaez, R. I. Rosales-Martinez, L. Narvaez-Hernandez, L. S. Hernandez-Hernandez and J. M. Miranda-Vidales, *Int. J. Electrochem. Sci.*, 10 (2015) 10003-10016.
32. C. T. Chen, J. J. Chang and W. C. Yeih, *Constr. Build. Mater*., 71 (2014) 35-43.
33. V. Feliu, J. A. González, C. Andrade and S. Feliu, *Corrosion Sci*., 40 (1998) 975-993.
34. M. Keddam, M. Krarti and C. Pallotta, *Corrosion*, 43 (1987) 454-458.
35. V. Rasanen and V. Penttala, *Cem. Concr. Res.*, 34 (2004) 813-820.
36. Q. Pu, L. H. Jiang, J. X. Xu, H. Q. Chu, Y. Xu and Y. Zhang, *Constr. Build. Mater*., 28 (2012) 519-524.
37. L. Li, A. A. Sagüés and N. Poor, *Cem. Concr. Res*., 29 (1999) 315-321.
38. F. Bjork and C. A. Eriksson, *Constr. Build. Mater*., 16 (2002) 535-542.
39. H. Xu, Y. Liu, W. Chen, R. G. Du and C. J. Lin, *Electrochim. Acta*, 54 (2009) 4067-4072.
40. B. Huet, V. L'Hostis, F. Miserque and H. Idrissi, *Electrochim. Acta*, 51 (2005) 172-180.
41. M. Moreno, W. Morris, M. G. Alvarez and G. S. Duffo, *Corrosion Sci*., 46 (2004) 2681-2699.
42. S. M. Abd El Haleem, E. E. Abd El Aal, S. Abd El Wanees and A. Diab, *Corrosion Sci*., 52 (2010) 3875-3882.